ELSEVIER

Nonlinear behavior of slender RC columns (1). Numerical formulation

Hyo-Gyoung Kwak *, Jin-Kook Kim

Department of Civil and Environmental Engineering, Korea Advanced Institute of Science and Technology, 373-1 Guseong-dong, Yuseong-gu, Daejeon 305-701, Korea

Abstract

This paper introduces an analytical model which can simulate the nonlinear behavior of slender reinforced concrete (RC) columns. The layer approach is adopted to determine the equilibrium conditions in a section and to consider the different material properties across the sectional depth effectively. The material nonlinearity including the cracking of concrete is taken into consideration, and geometric nonlinearity due to the P–Δ effect is taken into account by using the initial stress matrix. In advance, the creep deformation of concrete is described in accordance with a first-order algorithm based on the expansion of a degenerate kernel of the compliance function. To verify the analytical results, correlation studies with previous numerical results and experimental data are conducted, and numerous parameter studies are followed to discuss the structural responses of slender RC columns according to the changes in design variables. Finally, the necessity for a rigorous nonlinear analysis is emphasized for more accurate prediction of the ultimate resisting capacity of slender RC columns.
© 2005 Elsevier Ltd. All rights reserved.

Keywords: RC column; Ultimate resisting capacity; Slenderness ratio; P–Δ effect; Creep

1. Introduction

A reinforced concrete (RC) column, which is a primary structural member, is subjected to the axial force and bending moment which may be due to end restraint arising from the monolithic placement of floor beams and columns or due to eccentricity from imperfect alignment. Due to the combination of axial force and bending moment, the column section must be designed to ensure that the acting forces in a member exist inside the P–M interaction diagram representing the resisting capacity of the column. Recently, because of architectural aesthetics and efficiency in use of space, relatively slender columns have frequently been used in many

building structures, either throughout an entire building or in some parts of a structure, e.g., the exterior of buildings and the interior of lobbies. Moreover, the use of high strength steel and concrete has led to an increased use of slender members. However, as slender RC columns may fail due to not only material failure in a section but also instability of a structure, they require more rigorous numerical analyses which consider secondary effects such as the P–Δ effect and creep deformation of concrete in order to reserve their strength and serviceability.

There has been a lot of research on the behavior and design of slender RC columns. On the basis of the force equilibrium equation and the strain compatibility condition at a section, Bazant et al. [3,5] analytically calculated the resisting capacity of slender RC columns by assuming a deflection curve with a sinusoidal function. Material nonlinearity of steel and concrete was taken into

---
* Corresponding author. Tel.: +82 42 869 3621; fax: +82 42 869 3610.
  E-mail addresses: khg@kaist.ac.kr (H.-G. Kwak), glory95@kaist.ac.kr (J.-K. Kim).

account and an excellent discussion of slenderness effects on interaction diagrams was provided. Kim et al. [10,11] introduced a numerical method considering material and geometric nonlinearities by using the layer model and carried out an experimental study to verify the exactness of the algorithm they developed. Drysdale and Huggins [8] conducted experimental and analytical studies for both short-term and long-term behaviors of RC columns with relatively high slenderness ratio and discussed decrease of the ultimate resisting capacity due to the $P–\Delta$ effect and creep deformation of concrete. Recently, Yalcin and Saatcioglu [21] developed an analytical model that considers the influence of anchorage slip and plastic hinge length on the nonlinear behavior of RC columns.

In this paper, an analytical model to predict the resisting capacity of slender RC columns is proposed. The layer approach is adopted to simulate the different material properties across the sectional depth. Material nonlinearity due to the cracking of concrete and yielding of reinforcing bars, and geometric nonlinearity due to the $P–\Delta$ effect are taken into account. Concrete creep is evaluated by the first-order algorithm based on the expansion of the compliance function [9], and the aging effect of concrete properties is included in the evaluation. The validity of the numerical model proposed in this paper is established by comparing the analytical predictions with results from previous analytical studies [5,10], and numerical analyses for slender RC columns are conducted. On the basis of the numerical results obtained, the necessity of rigorous nonlinear analysis is emphasized for more accurate prediction of the ultimate resisting capacity of slender RC columns.

2. Structural behavior of slender RC columns

Generally, the ultimate compressive force P_0 and the ultimate bending moment M_0 for an RC column section are related to each other by means of an interaction diagram ($P–M$ interaction diagram). In the absence of second-order effects ($P–\Delta$ effect), as in very short columns, the cross-section would undergo proportional loading until reaching the material strength at point A of the cross-section interaction diagram (see Fig. 1). Slender columns, however, will follow the loading path up to point B where the material strength is reached. Point B is on the cross-section interaction diagram but is at a smaller axial load, P_{so}, than it would be if L/r were actually zero. Unlike a steel column, a concrete column accompanies relatively large time-dependent deformation, such as creep. This time-dependent deformation gradually increases the lateral deflection caused by the initial eccentricity e and the $P–\Delta$ effect, and finally decreases the ultimate resisting capacity and serviceability of slender RC columns.
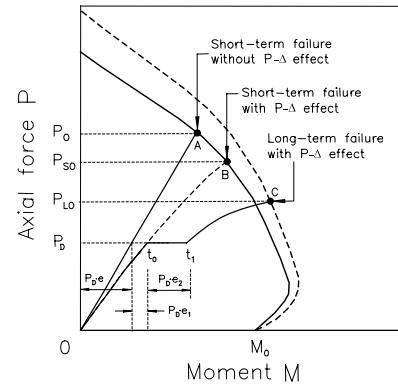

Fig. 1. Behavior of slender RC column.

In the case of an RC column with a relatively large slenderness ratio, instability failure, which means a failure before reaching the $P–M$ interaction diagram of an RC cross-section (the solid line envelope in Fig. 1), may occur. A typical description for the long-term failure is illustrated in Fig. 1. When an axial load P_D with initial eccentricity e acts on a slender RC column at $t = t_0$, the instantaneous lateral deflection will be e_1 due to second-order effects ($P–\Delta$ effect). Moreover, the creep deformation during $t_0 \sim t_1$ will increase the lateral deflection in spite of the absence of additional axial load. If an additional live load is applied at $t = t_1$, its increment terminates at point C, located outside the cross-section interaction diagram, because the strength for a live load applied after a period of creep under constant load P_D is usually higher than the short-term strength. The larger the column slenderness ratio, the greater is the reduction in the axial force resistance.

For not too slender columns, the failure occurs at points rather close to the material strength. For very slender columns, on the other hand, the failure occurs well within the cross-section interaction diagram because of a pronounced second-order effect. Referring to the structural behavior of RC columns, material nonlinearities of steel and concrete and time-dependent deformation of concrete are taken into account for more exact estimation of the ultimate resisting capacity of RC columns. Moreover, it needs to be assumed that the failure of RC columns occurs due to material failure only because the slenderness ratio in most RC columns designed in practice is smaller than the critical ratio that causes instability failure, even if the slenderness ratio ranges to a large value.

3. Modeling of material properties

3.1. Concrete

Based on the principle of superposition, total uniaxial concrete strain $\varepsilon_c(t)$ at any time t is assumed to be

composed of the mechanical strain $\varepsilon_c^m(t)$ caused by short-term service loads, and the nonmechanical strain $\varepsilon_c^{nm}(t)$ consists of creep strain $\varepsilon_c^{cr}(t)$ and shrinkage strain $\varepsilon_c^{sh}(t)$.

$$\varepsilon_c(t) = \varepsilon_c^m(t) + \varepsilon_c^{nm}(t) = \varepsilon_c^m(t) + \varepsilon_c^{cr}(t) + \varepsilon_c^{sh}(t). \qquad (1)$$

Shrinkage strain can be evaluated directly by utilizing the shrinkage models proposed in the design codes [1,7] since it is defined as the volume change that occurs independently of imposed stresses. On the other hand, creep is defined as an increase in strain under sustained stress. Introduction of an analytical model to calculate the creep strain is inquired, and many studies have been performed [4,9]. In this paper, the first-order algorithm based on expansion of creep compliance, proposed by Kabir and Scordelis [9], has been adopted because this model can simulate the stress history effectively in spite of its simplicity in application.

The increment of creep strain from time t_{n-1} to time t_n for uniaxial stress state can be expressed as follows [2,4]:

$$\Delta\varepsilon_n^c = \sum_{i=1}^m A_{i_{n-1}}\left(1 - e^{-\lambda_i \Delta t_n}\right), \quad A_{i_n} = A_{i_{n-1}}e^{-\lambda_i \Delta t_n} + a_i(\tau)\Delta\sigma_n, \qquad (2)$$

where $\Delta\varepsilon_n^c$ is the increment of creep strain, λ_i are inverse retardation times, $a_i(\tau)$ are constants depending on the age at loading τ, m is a number of time steps, and A_i with initial values $A_{i_1} = a_i(t_1) \cdot \Delta\sigma_1$ at $n = 1$ represent hidden state variables by which the effects of past time steps are considered.

Before starting the calculation of creep strain by Eq. (2), parameters such as m, $a_i(\tau)$ and λ_i must be determined. Since the use of the compliance function ($J(t,\tau) = 1/E(t) + C(t,\tau)$) in the form of a Dirichlet series induces some numerical difficulties caused by not considering a separate term to represent the instantaneous deformation, the creep compliance ($C(t,\tau)$) is used directly in this study, as shown in Eq. (3). Hence, $m = 4$ is taken, and the assumed corresponding retardation times are 8.0, 80.0, 800.0, and 8000.0, respectively. Besides, the values of $a_i(\tau)$ are determined by the method of least squares using Kabir's Dirichlet series creep compliance [9]. After determination of nonmechanical strain increments, the concrete stress at each layer corresponding to the mechanical strain can be calculated by using the stress–strain relation of concrete.

$$C(t,\tau) = \sum_{i=1}^m a_i(\tau) \cdot \left[1 - e^{-\lambda_i(t-\tau)}\right]. \qquad (3)$$

The response of RC columns under loads depends to a large extent on the stress–strain relation of the constituent materials and the magnitude of stress. Since concrete is used mostly in compression, the stress–strain relation in compression is of primary interest. Of many mathematical models currently used in the analysis of RC structures, the monotonic envelope curve introduced by Kent and Park and later extended by Scott et al. [18] is adopted in this paper because of its simplicity and computational efficiency. In this model, as shown in Fig. 2(a), the monotonic concrete stress–strain relation in compression is described by three regions, where ε_{co} is the concrete strain at maximum stress, K is a factor which accounts for the strength increase due to confinement, and Z is the strain softening slope.

On the other hand, it is assumed that concrete is linearly elastic in the tension region. Beyond the tensile strength, the tensile stress decreases linearly with increasing principal tensile strain (see Fig. 2(b)). Ultimate failure is assumed to take place due to cracking, when the principal tensile strain exceeds the value $\varepsilon_0 = 2 \cdot G_f/f_t \cdot \ln(3/b)/(3-b)$ in Fig. 2(b), where b is the element length. G_f is the fracture energy that is dissipated in the formation of a crack of unit length per unit thickness and is considered to be a material property. The value of ε_0 is derived from the fracture mechanics concept of equating the crack energy release with the fracture toughness of concrete G_f [12]. The experimental study by Welch and Haismen [20] indicates that for normal strength concrete, the value of G_f/f_t is in the range of 0.005–0.01 mm. If G_f and f_t are known from measurements, ε_0 can be directly determined from the equation in Fig. 2. More details for the concrete model can be found elsewhere [13].

3.2. Steel

Reinforcing steel is modeled as a linear elastic, linear strain hardening material with yield stress f_y. The reasons for this approximation are: (1) the computational convenience of the model; and (2) the behavior of RC

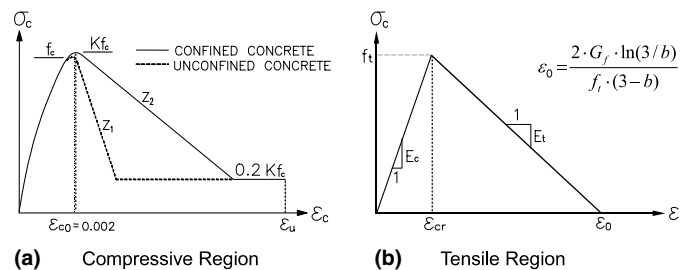**(a)**   Compressive Region   **(b)**   Tensile Region

Fig. 2. Stress–strain relation of concrete.

members is greatly affected by the yielding of reinforcing steel when the structure is subjected to a monotonic bending moment [17,19]. Thermal strain is the only non-mechanical strain expected for steel. However, it is not considered in this study, and thus the mechanical strain can be directly calculated from the total strain of steel $(\varepsilon_s(t) = \varepsilon_s^m(t))$.

4. Determination of neutral axis

In order to formulate the constitutive relationships in the section of an RC column, the following simplified assumptions have been made: (1) The section of an element is divided into imaginary layers to describe the different material properties; (2) plane sections remain plane to represent the linearity in the strain distribution on any section at any loading history; (3) a perfect bond between the concrete matrix and reinforcing bars is assumed; and (4) the constitutive materials are assumed to carry uniaxial stress only. In addition, shear deformation is not taken into account in the formulation because the shear effect is expected to be very small in slender RC columns.

Unlike a beam element subjected to a bending moment only, a column element is subjected to both axial force and bending moments so that the neutral axis of a column section cannot be calculated directly by the equilibrium condition of normal force only. To determine the neutral axis while considering bending effects, the mechanical strains of concrete (ε_c^m) and steel $(\varepsilon_s^m = \varepsilon_s^t)$ need to be partitioned into an axial strain $(\varepsilon_{ca}^m, \varepsilon_{sa}^t)$ and a bending strain $(\varepsilon_{cb}^m, \varepsilon_{sb}^t)$, as represented in Fig. 3.

Since the axial strain is constant across the section and the bending strain is zero at the neutral axis, the bending strains of concrete and steel at any layer can be calculated by $\varepsilon_{cb}^m = \varepsilon_c^m - \varepsilon_{ca}^m = \varepsilon_c^t - \varepsilon_c^{nm} - \varepsilon_{ca}^m$ and $\varepsilon_{sb}^t = \varepsilon_s^t - \varepsilon_{sa}^t$, respectively. Based on the assumed neutral axis, the stress corresponding to the mechanical bending strain can be calculated from the stress–strain curves of the constitutive materials, and iterations using the bisection method are repeated until errors for the axial force and bending moment calculated by the axial strain and bending strain are within the given tolerances [14].

In addition, time rate in a stress increment has been considered. If a stress increment $\Delta\sigma_c(t_0)$ is introduced at time t_0 and sustained without a change in magnitude, the time variation of strain in concrete follows the continuous line ABC in Fig. 4, and the total strain at time t, instantaneous plus creep, can be represented by

$$\Delta\varepsilon_c^{cr}(t) = \frac{\Delta\sigma_c(t_0)}{E_c(t_0)}(1 + \phi), \tag{4}$$

where $\phi = \phi(t, t_o)$ is the creep coefficient.

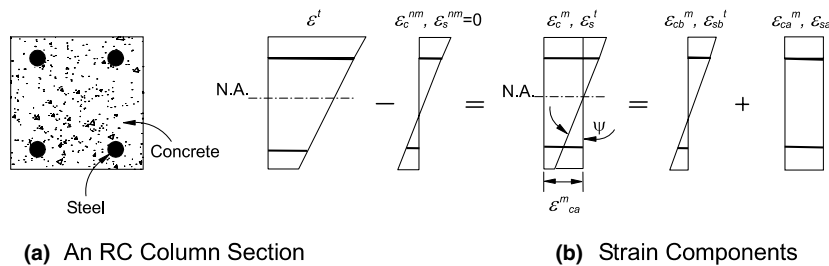**(a)** An RC Column Section   **(b)** Strain Components
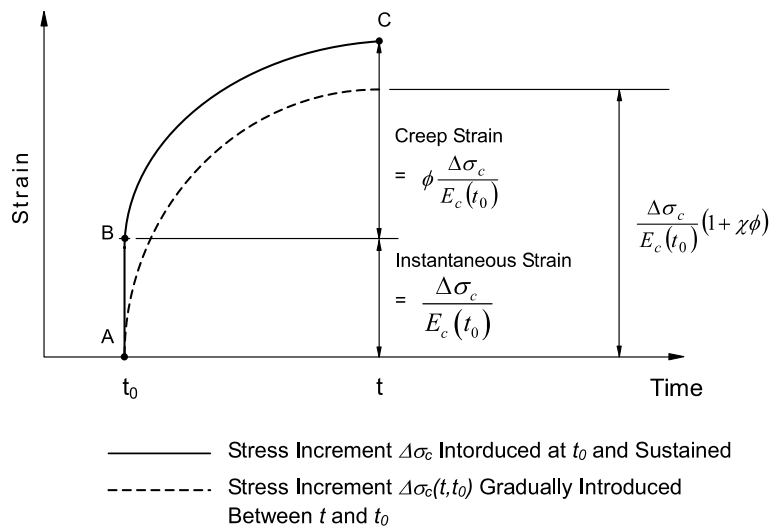
Fig. 3. Strain components at a section.

Fig. 4. Time variation of strain caused by a stress increment $\Delta\sigma_c$.

On the other hand, when a stress increment $\Delta\sigma_c(t,t_0)$ is gradually introduced between t_0 and t, the strain variation with time can be represented by the dashed line in Fig. 4. The total strain produced during the period $t_0 \sim t$ can be obtained by

$$\Delta\varepsilon_c^{cr}(t,t_0) = \frac{\Delta\sigma_c(t_0,t_0)}{E_c(t_0)}(1 + \chi\phi), \qquad (5)$$

where χ is the concrete aging coefficient which accounts for the effect of aging on the ultimate value of creep for stress increments or decrements occurring gradually after the application of the original load. It is found that an average value of $\chi = 0.82$ can be used for most practical problems where the creep coefficient lies between 1.5 and 3.0 and t_0 is greater than 5 days. An approximate value of 0.8 has frequently been used for χ, and the same value of $\chi = 0.82$ is adopted in this study [16].

5. Construction of equilibrium equation

Based on the assumed displacement field formulation, all the constitutive equations including the element stiffness matrix are derived. As shown in Fig. 5, the nodal displacement vectors of a two-dimensional beam element in its local coordinate system can be expressed by $\boldsymbol{u} = \{u_1, u_2\}^T$, $\boldsymbol{v} = \{v_1, v_2\}^T$, and $\boldsymbol{\theta} = \{\theta_1, \theta_2\}^T$ and the nodal displacements of an element may be expressed as the column vector $\boldsymbol{r} = \{\boldsymbol{u}, \boldsymbol{v}, \boldsymbol{\theta}\}^T$.

Assuming that the independent axial displacement $U_0(x)$ varies linearly with x, and that the small rotation θ_i at each node can be calculated by derivation of the vertical displacement v_i with respect to x, the displacements, $U_0(x)$ and $V(x)$ at any point within the element, can be represented by

$$U_0(x) = \phi \cdot \boldsymbol{u}, \quad V(x) = \psi \cdot \begin{Bmatrix} \boldsymbol{v} \\ \boldsymbol{\theta} \end{Bmatrix}, \qquad (6)$$

where $\phi = [(1 - p), p]$ and $\psi = [(1 - 3p^2 + 2p^3), (3p^2 - 2p^3), L(p - 2p^2 + p^3), L(-p^2 + p^3)]$ represent the displacement shape functions, and the nondimensional parameter p denotes x/L, that is, the position along the axis of the beam element.

Then, by adopting the plane section hypothesis, the x displacement $U(x)$ at any point can be written by the relation of $U(x,y) = U_0(x) - y \cdot dV(x)/dx = \phi \cdot \boldsymbol{u} -$

$y\psi_{,x}\begin{Bmatrix} \boldsymbol{v} \\ \boldsymbol{\theta} \end{Bmatrix}$. Hence, x displacement $U(x,y)$ and y displacement $V(x,y)$ may be expressed in terms of the displacement column vector $\boldsymbol{r}$

$$U(x,y) = [\phi, -y\psi_{,x}] \cdot \boldsymbol{r}, \quad V(x) = [0, \psi] \cdot \boldsymbol{r}, \qquad (7)$$

where $\psi_{,x}$ means the first order derivative of ψ with respect to x.

In addition, the axial strain $\varepsilon(x,y)$ can be defined by

$$\varepsilon(x,y) = \frac{dU(x,y)}{dx} + \frac{1}{2}\left(\frac{dV(x)}{dx}\right)^2, \qquad (8)$$

where the second term represents the nonlinear displacement effect.

When a finite change in the joint displacement $\Delta\boldsymbol{r}$ occurs, corresponding changes in the strain $\Delta\varepsilon$ can be expressed by

$$\begin{aligned} \Delta\varepsilon &= \frac{d\Delta U}{dx} \\ &= [\phi_{,x}, -y\psi_{,xx}] \cdot \Delta\boldsymbol{r} + \frac{1}{2}\Delta\boldsymbol{r}^T \cdot [0, \psi_{,x}]^T \cdot [0, \psi_{,x}] \cdot \Delta\boldsymbol{r} \\ &= \boldsymbol{B} \cdot \Delta\boldsymbol{r} + \frac{1}{2}\Delta\boldsymbol{r}^T \cdot \boldsymbol{c}^T \cdot \boldsymbol{c} \cdot \Delta\boldsymbol{r}, \end{aligned} \qquad (9)$$

where $B = [\phi_{,x}, -y\psi_{,xx}] = [-1/L, 1/L, y(1 - 2p)(6/L^2), y(-1 + 2p)(6/L^2), y(2 - 3p)(2/L), y(1 - 3p)(2/L)]$. Moreover, the incremental strain–displacement relationship of $d\varepsilon = \boldsymbol{B} \cdot d\boldsymbol{r} + d\boldsymbol{r}^T \cdot \boldsymbol{c}^T \cdot \boldsymbol{c} \cdot \Delta\boldsymbol{r} = d\boldsymbol{r}^T \cdot (\boldsymbol{B} + \boldsymbol{c}^T \cdot \boldsymbol{c} \cdot \Delta\boldsymbol{r})$ can be developed by taking the differential from Eq. (9).

Applying the virtual work principle of $d\boldsymbol{r}^T \cdot (R^j + \Delta R^j) = \int_V d\varepsilon \cdot (\sigma + \Delta\sigma) dV$ to a finite element on the basis of the virtual displacement $d\boldsymbol{r}$ and neglecting a higher order incremental term, the incremental of nodal force vector $\Delta\boldsymbol{R}^j$ applied at node j can be written from Eq. (9) as

$$\begin{aligned} \Delta\boldsymbol{R}^j &= \int_V \boldsymbol{B}^T \Delta\sigma \, dV + \int_V \boldsymbol{c}^T \sigma \boldsymbol{c} \, dV \cdot \Delta\boldsymbol{r} \\ &= \int_V \boldsymbol{B}^T E(d\varepsilon^t - d\varepsilon^{nm}) \, dV + \int_V \boldsymbol{c}^T \sigma \boldsymbol{c} \, dV \cdot \Delta\boldsymbol{r} \\ &= \left[\int_V \boldsymbol{B}^T E \boldsymbol{B} \, dV + \int_V \boldsymbol{c}^T \sigma \boldsymbol{c} \, dV\right] \cdot \Delta\boldsymbol{r} \\ &\quad - \int_V \boldsymbol{B}^T E \, d\varepsilon^{nm} \, dV, \end{aligned} \qquad (10)$$

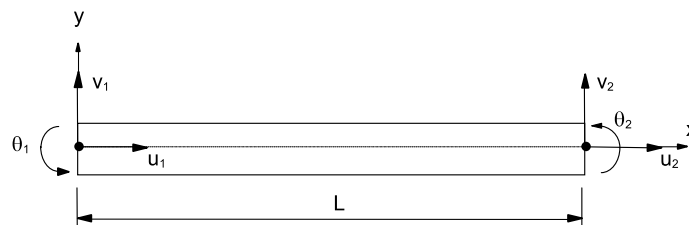where E is the tangent modulus of constitutive material.

Fig. 5. Displacement components in a beam element.

Finally, the equilibrium equations can be rewritten in differential form as

$$\mathbf{dR} = \mathbf{dR}^j + \mathbf{dR}^{\mathrm{nm}} = [\mathbf{K}] \cdot \mathbf{dr}, \tag{11}$$

where

$$[\mathbf{K}] = [\mathbf{K}_e] + [\mathbf{K}_g] = \int_V \mathbf{B}^{\mathrm{T}} E \mathbf{B} \, \mathrm{d}V + \int_V \mathbf{c}^{\mathrm{T}} \sigma \mathbf{c} \, \mathrm{d}V,$$

$$[\mathbf{K}_e] = \int_V \mathbf{B}^{\mathrm{T}} E \mathbf{B} \, \mathrm{d}V, \quad [K_g] = \int_V \mathbf{c}^{\mathrm{T}} \sigma \mathbf{c} \, \mathrm{d}V,$$

$$\mathbf{dR}^{\mathrm{nm}} = \int_V \mathbf{B}^{\mathrm{T}} E \, \mathrm{d}\varepsilon^{\mathrm{nm}} \, \mathrm{d}r,$$

$$[K_e] = \begin{bmatrix} EA/L & -EA/L & 0 & 0 & 0 & 0 \\ & EA/L & 0 & 0 & 0 & 0 \\ & & 12EI/L^3 & -12EI/L^3 & 6EI/L^2 & 6EI/L^2 \\ & & & 12EI/L^3 & -6EI/L^2 & -6EI/L^2 \\ & \text{sym.} & & & 4EI/L & 2EI/L \\ & & & & & 4EI/L \end{bmatrix}, \tag{12}$$

$$[K_g] = \begin{bmatrix} 0 & 0 & 0 & 0 & 0 & 0 \\ & 0 & 0 & 0 & 0 & 0 \\ & & 6P/5L & -6P/5L & P/10 & -P/10 \\ & & & 6P/5L & -P/10 & -P/10 \\ & \text{sym.} & & & 2PL/15 & -PL/30 \\ & & & & & 2PL/15 \end{bmatrix}, \tag{13}$$

while calculating the elastic stiffness $[K_e]$ and the geometric stiffness $[K_g]$, the value of E at each layer is assumed to be held constant along the element length, and thus the volume integration in Eq. (10) can be represented by the inner product of the line integration along the element length and the area integration across the sectional depth. Moreover, since the layer approach is employed, wherein a typical section is divided into imaginary layers, the sectional stiffness terms of EA and EI in Eq. (12) can be evaluated by summation over all layers, i.e., $EA = \int_A E \, \mathrm{d}A = \sum_{i=1}^{n_c} E_{c_i} A_{c_i} + \sum_{i=1}^{n_s} E_{s_i} A_{s_i}$ and $EI = \int_A E y^2 \, \mathrm{d}A = \sum_{i=1}^{n_c} E_{c_i} y_{c_i}^2 A_{c_i} + \sum_{i=1}^{n_s} E_{s_i} y_{s_i}^2 A_{s_i}$, where n_c and n_s denote the number of concrete and steel layers respectively, A_i and E_i are the sectional area and elastic modulus of ith layer, y_i is the distance from the centroid, and P refers to the applied force.

6. Solution algorithm

Every nonlinear analysis algorithm consists of four basic steps: the formation of the current stiffness matrix, the solution of the equilibrium equations for the displacement increments, the state determination of all elements in the model, and a convergence check. These steps are presented in some detail in the flow diagr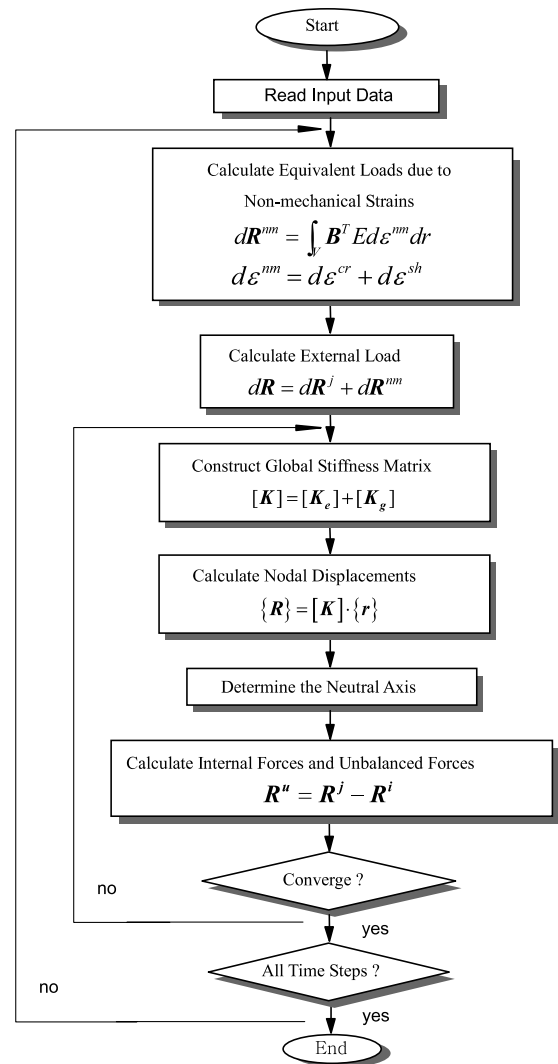am of Fig. 6. Since the global stiffness matrix of the structure depends on the displacement increments, the solution of the equilibrium equations is typically accompanied by an iterative method through the convergence check. The nonlinear solution scheme selected in this paper uses the tangent stiffness matrix at the beginning of each load step and each time step in combination with a constant stiffness matrix during the subsequent correction phase, that is, an incremental-iterative method.

The criteria for measuring the convergence of the iterative solution are generally based on the accuracy of satisfying the global equilibrium equations or on the accuracy of determining the total displacements. The accuracy of satisfying the global equilibrium is controlled by the magnitude of the unbalanced nodal forces. Hence the convergence criteria for the unbalanced nodal forces are used in this paper, and these can be expressed as

$$|F_{\mathrm{unbal.}}^{\max}| \leqslant \mathrm{Tol.}_F, \quad |M_{\mathrm{unbal.}}^{\max}| \leqslant \mathrm{Tol.}_M, \tag{14}$$

Fig. 6. Solution procedure.

where $|F_{unbal.}^{max}|$ and $|M_{unbal.}^{max}|$ are the absolute values of the maximum unbalanced axial force and bending moment, respectively, and $Tol._F$ and $Tol._M$ are the specified tolerances corresponding to the axial force and bending moment. $Tol._F = Tol._M = 0.01$ are taken in this study, and more details for the solution procedures can be found elsewhere [14].

7. Analytical and experimental verification

7.1. Short-term loading

The experimental results from several hinged RC columns tested by Kim and Yang [11] are used to investigate the validity of the analytical model proposed in this paper. More details from the material properties used in the experimental procedure for each specimen can be found elsewhere [11].

The ultimate loads of columns measured experimentally are compared with those obtained by the analytical model in Table 1 in which the third column shows two test results measured from two specimens with the same specification for each slenderness ratio. The good agreements for the individual columns, regardless of the compressive strength of concrete and the slenderness ratio, lead to the conclusion that the ultimate loads of hinged RC columns can be accurately predicted by the proposed numerical model. In addition, Fig. 7 representing a relation between the axial force and lateral deflection at the mid-span, shows that the proposed numerical model not only gives accurate predictions for the ultimate load but also effectively simulates the nonlinear behavior of simply supported slender RC columns as the axial force increases from zero to its ultimate value.

Table 1
Comparison of computed ultimate strength of RC columns with test results from Kim and Yang [11]

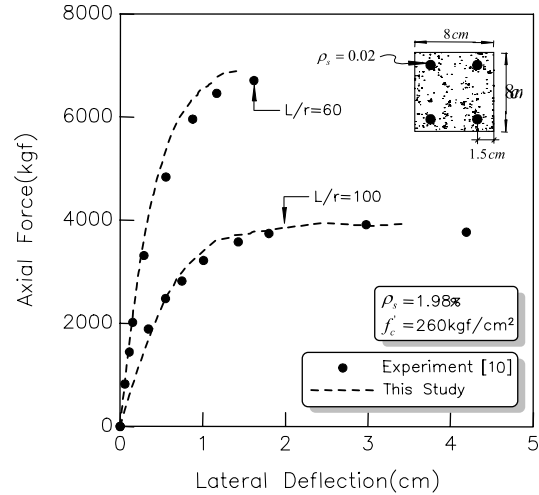| f_c' (kgf/cm^2)	L/r	Test results $P_{u,t}$ ($\times 10^3$ kgf) (Kim et al.)	Analysis results $P_{u,a}$ ($\times 10^3$ kgf) (This study)	$P_{u,a}/P_{u,t}$
259.9	60	6493	6600	1.02
		6697		0.99
	100	3894	3780	0.97
		3568		1.06
647.3	60	10479	10400	0.99
		11570		0.90
	100	4608	4840	1.05
		4852		1.00
878.7	60	12446	11840	0.95
		12610		0.94
	100	5535	5520	1.00
		5596		0.99

Fig. 7. Comparison of analytical model with test results.

The second group of specimens used to validate the proposed analytical model is a series of columns with a width × depth of 20 cm × 30 cm. These columns were tested by Chuang and Kong [6]. More details of the material properties as well as the configuration of the specimens can be found elsewhere [6]. From Table 2, which shows the experimental results and the analytical predictions, it can be seen that the proposed numerical model accurately predicts the ultimate load regardless of the eccentricity ratio.

An additional comparison with numerical calculations introduced by Bazant et al. [3,5] is conducted to verify the accuracy of the proposed numerical model. The steel ratio and cross-section dimensions of the selected columns with slenderness ratios of $L/r = 10$, 70 and 100 are represented in Fig. 8. The same material properties of concrete and steel as those in the previous analytical study are used and have the following values: $f_c' = 5000$ psi (352 kgf/cm^2), $E_s = 29 \times 10^6$ psi (2.04×10^6 kgf/cm^2) and $f_y = 60\,000$ psi (4220 kgf/cm^2).

For the design of slender RC columns, ACI318 [1] recommends a simple approximate formula based on the moment magnification factor. When a column is subjected to ultimate loads of P_u and M_u, the load and moment used in the design of the column section are assumed to be P_u and $\delta \cdot M_u$, where δ is the moment magnification factor, and is calculated from $\delta = C_m/(1 - P_u/\phi_k \cdot P_{cr}) \geq 1$; P_{cr} is the elastic buckling load; and C_m is an equivalent uniform moment diagram factor. Note that $C_m = 1$ for the columns used in this example.

Moreover, as mentioned in a previous study [15], the stiffness reduction factor ϕ_k designed to consider the inevitable random variability of the materials has not been incorporated for the purpose of comparison with the numerical results (i.e. $\phi_k = 1.0$ is assumed).

As shown in Fig. 8, the results from the proposed numerical model are in good agreement with those

Table 2
Comparison of computed ultimate strengths of RC columns with test results from Chuang and Kong [6]

| Specimen	L/r	e/h	ρ (%)	Test results $P_{u,t}$ ($\times 10^3$ kgf)	Analysis results $P_{u,a}$ ($\times 10^3$ kgf)	$P_{u,a}/P_{u,t}$
A-17-0.25	58.9	0.25	3.27	120.3	123.5	1.03
A-18-0.25	62.4			110.1	113.8	1.03
A-19-0.25	65.8			121.8	107.3	0.88
A-17-0.50	58.9	0.50		91.9	92.0	1.00
A-18-0.50	62.4			86.7	84.0	0.97
A-19-0.50	65.8			83.1	82.0	0.99
B-17-0.25	58.9	0.25	1.34	110.8	106.0	0.96
B-18-0.25	62.4			100.7	100.0	0.99
B-19-0.25	65.8			106.6	92.0	0.86
B-17-0.50	58.9	0.50		48.8	50.0	1.02
B-18-0.50	62.4			48.8	50.0	1.02
B-19-0.50	65.8			47.1	49.0	1.04
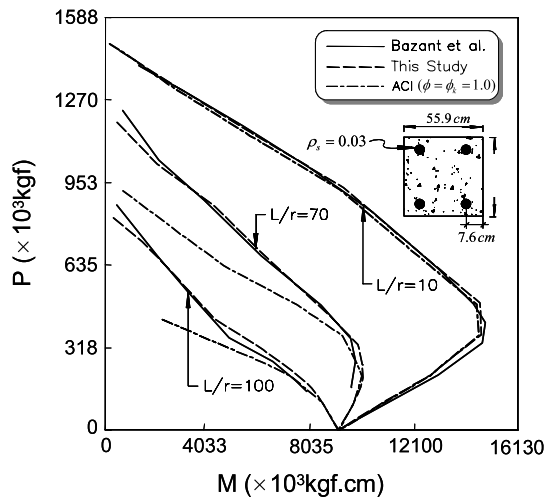
Fig. 8. Failure envelopes for pin-ended RC columns.

obtained by Bazant and Xiang [5], and leading to the conclusion that the ultimate loads of slender RC columns can be accurately predicted by the proposed numerical model. Fig. 8 also leads to the following conclusions: (1) As the slenderness ratio increases, the difference between the ACI strength interaction curve and the proposed model gradually increases; (2) the ACI method may underestimate the resisting capacity of slender RC columns; and (3) the ACI method does not achieve a uniform safety margin, defined in this study as the uniform difference between the results predicted by the ACI method and the results calculated by a rigorous analysis over the entire interaction diagram for columns with $L/r = 70$ and 100.

7.2. Long-term loading

To verify the accuracy of the proposed numerical model for long-term behavior, correlation studies between analytical and experimental results by Drysdale and Huggins [8] are conducted. The geometry and cross-section dimensions of the tested columns are represented in Fig. 9, and those columns have a slenderness ratio of $L/r = 107$. Moreover, the following material properties, which have the same values with those used in the experiments, are used: $f'_c = 4000$ psi (282 kgf/cm^2), $E_s = 29 \times 10^6$ psi (2.04$\times 10^6$ kgf/cm^2), and $f_y = 56\,000$ psi (3940 kgf/cm^2). To trace the time-dependent behavior of RC columns, creep and shrinkage of concrete are considered with the aging effect of concrete, and an ultimate creep coefficient of $c_u = 3.0$ and an ultimate shrinkage strain of $\varepsilon_{sh}^{\infty} = 600 \times 10^{-6}$ are used on the basis of the ACI model.

Fig. 9 shows a plot of P_{ou}/P_{ut} versus β_d where $\beta_d = P_D/(P_D + P_L)$ = ratio of dead load to total load, P_{ou} = short-term failure load, and P_{ut} = long-term failure load. When an RC column is subjected to a small sustained load, which means that β_d has a small value, the points of failure caused by the subsequent sudden overload generally indicate a substantial increase in strength. This phenomenon, however, is almost nonexistent in the tests of Drysdale et al. because drying
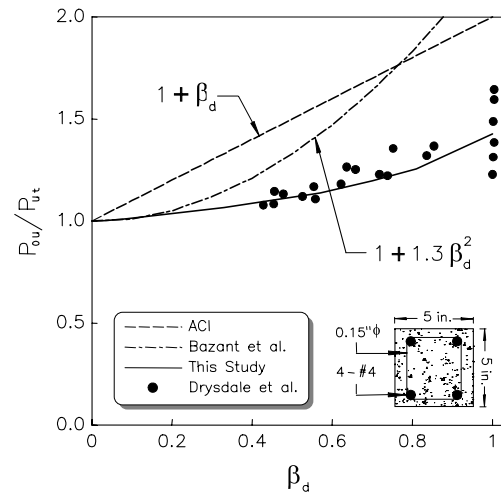

Fig. 9. Long-term resistance of RC columns.

prevents the increase of concrete strength due to hydration. This means that the analytical results may represent lower values of P_{ou}/P_{ut} than those from the experimental data along the whole range of β_d because the increase in concrete strength can accurately be considered in the numerical analyses by implementing the age effect. In this aspect, the two models proposed by the ACI and Bazant et al. give slightly conservative results and underestimate the resisting capacity of slender RC columns as β_d increases. In advance, since the dead load takes possession of 50% of the total design load in most RC columns ($\beta_d \geqslant 0.5$), direct application of the ACI model or the Bazant model may result in a conservative design.

On the other hand, the numerical results from the proposed analytical model agree well with the experimental results. Especially at $\beta_d = 1$, the numerical result shows 30% reduction in the ultimate resisting capacity for the axial load. This coincides well with the experimental results, which represent reductions ranging from 20% to 40%.

8. Numerical analyses

8.1. Short-term loading

The ultimate resisting capacity of slender RC columns is affected by many variables in addition to the compressive strength of concrete, such as the slenderness ratio, steel ratio, eccentricity, etc. In order to isolate the effects of these variables, a parametric study is conducted. The same cross-section dimensions as those used in the analytical verification under short-term loading are used (see Fig. 10). Two values of steel ratio ($\rho_s = 0.03$ and 0.08) are investigated and the slenderness ratio is limited to a maximum $L/r = 70$, because the slenderness ratio of RC columns generally used in design practice is less than 70. The following material proper-

ties are assumed: $f_c' = 360\ \mathrm{kgf/cm^2}$, $E_s = 2.1 \times 10^6\ \mathrm{kgf/cm^2}$ and $f_y = 4350\ \mathrm{kgf/cm^2}$. The resulting strength interaction curves in terms of primary bending moments are given in Fig. 10.

As shown in Fig. 10, which represents the relation between the axial force and the primary bending moment, the P–Δ effect appears more significant as the steel ratio decreases. This seems to arise from the fact that columns with relatively small steel ratios have smaller bending stiffnesses, EI, at the post-cracking state, and this leads to an increase in the lateral deflection and accompanying the P–Δ effect. On the other hand, the P–Δ effect gradually disappears as the slenderness ratio converges to zero, so that a minor influence of the steel ratio on the P–Δ effect appears in columns with low slenderness ratios (i.e., $L/r \leqslant 30$). This effect also disappears when the applied axial force P becomes zero. More details related to the P–Δ effect can be found in the companion paper.

Fig. 11 shows the structural response of slender RC columns according to changes in the compressive strength of concrete. A more significant decrease of the ultimate resisting capacity with an increase of the slenderness ratio appears in the RC columns using concrete with relatively high compressive strength. Since the stress–strain relation of concrete represents more brittle behavior as the compressive strength increases, a slender high strength concrete column has a relatively small energy absorption capacity when it is subjected to a large lateral deflection accompanied by the P–Δ effect. This is why a significant decrease of the ultimate resisting capacity occurs in the high strength concrete column. The obtained results also show that the use of high strength concrete in slender RC columns is not as effective as in short columns.

8.2. Long-term loading

In order to study the long-term behavior of slender RC columns, time-dependent analyses using the
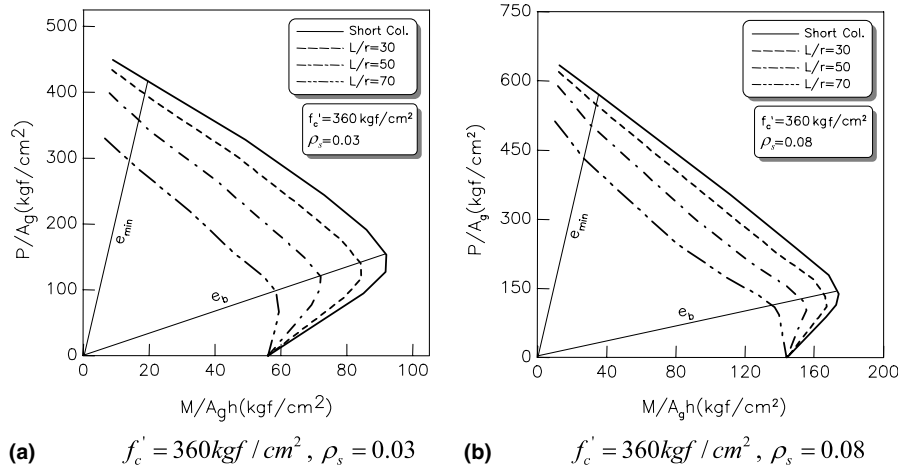

Fig. 10. P–M interaction diagrams of RC columns in accordance with the steel ratio.

(a) $f_c' = 360\ kgf/cm^2$, $\rho_s = 0.03$

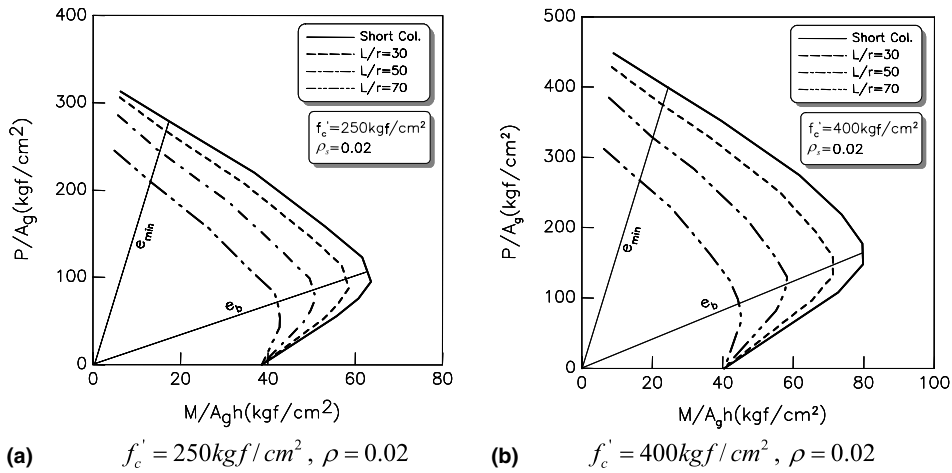(b) $f_c' = 360\ kgf/cm^2$, $\rho_s = 0.08$

Fig. 11. *P–M* interaction diagrams of RC columns in accordance with the compressive strength of concrete.

proposed model are conducted in the case of $\beta_d = 1$ because this case represents the most severe decrease in the ultimate resisting capacity for the axial load (see Fig. 9). The cross-section dimensions and material properties are the same as those used in the short-term loading case. Figs. 12 and 13 show the *P–M* interaction diagrams, which represent the relation between the axial force and the primary bending moment.
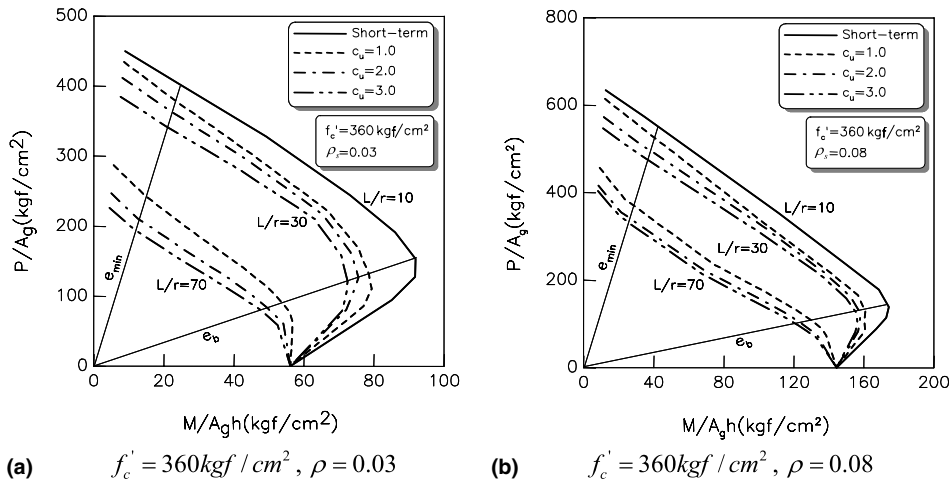

Fig. 12. *P–M* interaction diagrams of RC columns in accordance with the steel ratio.
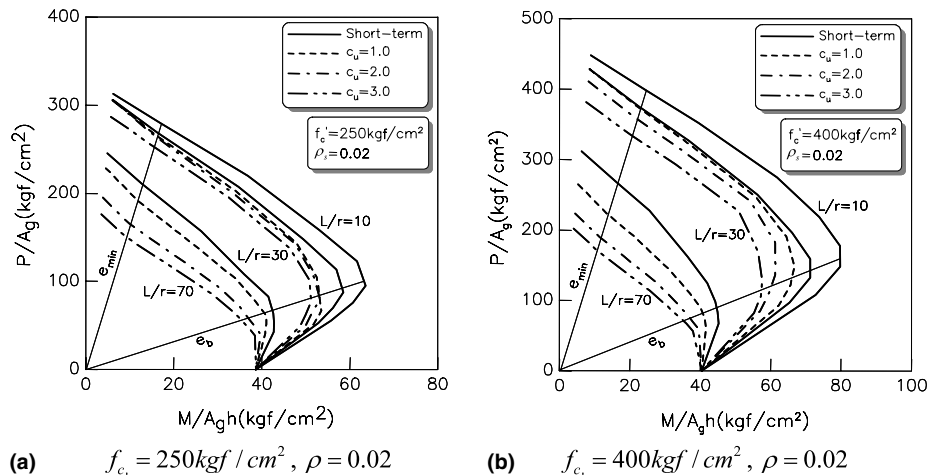

Fig. 13. *P–M* interaction diagrams of RC columns in accordance with the compressive strength of concrete.

As shown in Fig. 12, greater strength reduction due to the creep deformation of concrete appears in RC columns with relatively small reinforcement because the creep deformation in an RC section increases as the steel ratio decreases and larger creep deformation accompanies greater increase of the lateral deformation. In advance, this figure shows that more significant strength reduction due to creep deformation occurs in RC columns with larger slenderness ratios, and this tendency seems to be maintained always, regardless of changes in the variables. Fig. 13 also shows a decrease of the ultimate resisting capacity of RC columns according to the creep of concrete. It can be seen that the strength reduction due to the creep effect is increased proportionally to the compressive strength of concrete. Moreover, from a comparison of Figs. 12 and 13 with Figs. 10 and 11 for the short-term loading case, it can be found that all the characteristics for the resisting capacity of RC columns represented in short-term loading are maintained in the long-term behavior.

9. Conclusions

A numerical model to simulate the nonlinear behavior of slender RC columns considering the long-term deformations of concrete is presented in this paper, and the proposed model is verified by comparison with results from previous analytical and experimental studies. Moreover, on the basis of the numerical results in this limited investigation, the following conclusions are obtained: (1) the use of high-strength concrete in slender RC columns is not as effective as in short columns since the resisting capacity is significantly decreased in high-strength concrete columns; and (2) an increase of the steel ratio leads to a relatively small decrease in the ultimate resisting capacity of slender RC columns and improves the structural behavior under short-term and long-term loading.

Since the nonlinear behavior of slender RC columns is dominantly affected by many design variables such as the slenderness ratio, steel ratio, compressive strength of concrete, eccentricity and the magnitude of ultimate creep coefficient, etc., sophisticated numerical methods considering material and geometric nonlinearities will play an increasingly important role and will become the standards for final design checks. Nevertheless, the introduction of a simple design formula that can be effectively used in practice to determine an initial section of slender RC columns may be required because the design formulas noted in the current design codes still have some limitations in considering numerous design variables and they give slightly conservative results for slender RC columns.

References

[1] ACI Committee 318 Building Code Requirements for Reinforced Concrete (ACI 318–99). Detroit: American Concrete Institute; 1999.
[2] ASCE. State-of-art report on finite element analysis of reinforced concrete. New York: American Society of Civil Engineers; 1982.
[3] Bazant ZP, Cedolin L, Tabbara MR. New method of analysis for slender columns. ACI Struct J 1991;88(4):391–401.
[4] Bazant ZP, Wu ST. Dirichlet series creep function for aging concrete. J Eng Mech ASCE 1973;99(EM2):367–87.
[5] Bazant ZP, Xiang Y. Inelastic buckling of concrete column in braced frame. J Struct Eng 1997;123(5):634–42.
[6] Chuang EH, Kong FK. Large-scale tests on slender, reinforced concrete columns. Struct Eng 1997;75(4/5):410–6.
[7] Comite Euro-International du Beton CEB-FIP Model Code. London: Thomas Telford Service; 1993.
[8] Drysdale RG, Huggins MW. Sustained biaxial load on slender concrete columns. J Struct Div, ASCE 1971;97(No. ST5).
[9] Kabir AF, Scordelis AC. Nonlinear analysis of reinforced concrete panels, slabs and shells for time dependent effects. Report No. UC–SEEM 76–6. Berkeley: University of California; 1976.
[10] Kim JK, Lee SS. The behavior of reinforced concrete columns subjected to axial force and biaxial bending. Eng Struct 2000;22(11):1518–28.
[11] Kim JK, Yang JK. Buckling behaviour of slender high-strength concrete columns. Eng Struct 1995;17(1):39–51.
[12] Kwak HG, Filippou FC. Finite element analysis of reinforced concrete structures under monotonic loads. Report No. UCB/SEMM-90/14. Berkeley: University of California; 1990.
[13] Kwak HG, Kim SP. Bond-slip behavior under monotonic uniaxial loads. Eng Struct 2001;23(3):298–309.
[14] Kwak HG, Seo YJ. Long-term behavior of composite girder bridges. Comput Struct 2000;74(5):583–99.
[15] Mirza SA, Lee PM, Morgan DL. ACI stability resistance factor for RC columns. J Struct Eng, ASCE 1987;113(9):1963–1976.
[16] Neville AM, Dilger WH, Brooks JJ. Creep of plain and structural concrete. London and New York: Construction Press; 1982.
[17] Ngo D, Scordelis AC. Finite element analysis of reinforced concrete beams. ACI 1967;64(3):152–63.
[18] Scott BD, Park R, Priestley MJN. Stress–strain behavior of concrete confined by overlapping hoops at low and high strain rates. ACI 1982;79(1):13–27.
[19] Vedo A, Ghali A. Moment–curvature relation of reinforced concrete slabs. J Struct Div, ASCE 1977;103(3):515–31.
[20] Welch GB, Haisman B. Fracture toughness measurements of concrete. Report No. R42. Sydney: University of New South Wales; 1969.
[21] Yalcin C, Saatcioglu M. Inelastic analysis of reinforced concrete columns. Comput Struct 2000;77(5):539–55.